2024

Performance Comparison of a Residential Split-System Heat Pump Powered on AC versus DC Power

Aaron Harron Patrick Farha
afarha@purdue.edu

Davide Ziviani
dziviani@purdue.edu

Kevin James Kircher
kkirche@purdue.edu

Eckhard A. Groll
groll@purdue.edu

Performance Comparison of a Residential Split-System Heat Pump Powered on AC versus DC Voltage

A. H. P. Farha[1*], D. Ziviani[1], K. Kircher[1], E. A. Groll[1]

[1]Ray W. Herrick Laboratories
Purdue University
West Lafayette, IN 47907, USA

* Corresponding Author

ABSTRACT

Powering the world on DC voltage will be paramount to the future of renewable energy integration as most distributed energy systems are DC-driven (PV panels, batteries, etc.). Additionally, most residential appliances and devices typically run on DC voltage. Therefore, cutting out conversion losses due to AC-DC rectification has the potential for enhancing system efficiency, increasing reliability, and reducing points of failure. In building applications, space conditioning can sometimes account for up to 40% of the energy consumed. With the electrification of heating becoming more prevalent, it is thus necessary to rethink how these devices can be powered in a more efficient manner. The objective of the present study is to elucidate trends in the steady state performance of a variable speed residential split-system Air Source Heat Pump (ASHP) by comparing its performance on AC versus DC power sources in both heating and cooling test modes as prescribed by AHRI Standard 210/240. As a part of this study, a thermodynamic model and experimental results are presented. Findings indicate that the system COP is slightly improved (+2-3%) at full load conditions and worse at part load conditions (-3-5%). Future work will investigate dynamic testing of the DC-driven heat pump in a real home with a DC Nanogrid.

1. INTRODUCTION

Nearly half of all residential power consumption is due to space heating and cooling (EIA-1, 2023). Efforts aimed at increasing the electrification of heating and cooling technologies in buildings will cause major strain on the future of the US power grid. The US Department of Energy has projected that between 2023 and 2030, more than 200 GW of peak demand will have to be met (DOE, 2023). Adding to this issue is the necessary transition to a clean and renewable energy grid. However, renewables are often plagued with their own set of issues such as intermittent supply in solar and wind, transmission losses, and lack of sufficient battery technology. Solar and wind power are entirely dependent on weather conditions meaning their power production is non-controllable. Batteries are a way to take advantage of excess production when possible and store it for when it's needed, and although the technology is rapidly improving, it is unfortunately still not at the capability to supply sufficient long-term storage. Additionally, transmission losses often arise with the addition the need for converting DC to AC power for these DERs since solar is natively DC power, and wind power often has to be converted from AC generation to DC and back to AC so it can correctly interface with the power grid at 50 or 60 Hz. Virtual Power Plants (VPPs) which constitute an aggregation of DERs coordinated for optimal grid operation could be a potential solution to match the load in a decentralized approach (Downing, 2023). A VPP could take the form of building-to-grid services with an aggregation of many buildings (i.e. enabling flexibility to reduce demand on the grid), or it could even mean having standby power plants to sufficiently power a small amount of buildings. This indicates that the way that energy is produced *and* consumed must be considered in tandem. Microgrids could be one such asset to increase the resilience and reliability of the power grid. Controllable microgrids could help to improve the resiliency of the grid under extreme weather events since they can quickly be switched to an islanding mode of operation before there is an outage (Liu, 2016). Networked microgrids are also promising in building a robust infrastructure for the grid, but a key issue is that most generation sources are inverter-based for microgrids (solar, wind, electrical storage, etc.), requiring advanced controls strategies such as frequency-watt droop methods (Chen, 2020) to better integrate these resources with the current power grid infrastructure.

Alternating Current (AC) has been standard for power distribution for decades, however a significant portion of devices powered in a home are powered on Direct Current (DC); batteries, TVs, lights, and most motors are all DC powered to name a few. Solar panels, which naturally produce DC voltage, are also currently the cheapest form of

electricity on the market with widespread adoption for residential rooftop installations increasing year-over-year (EIA-2, 2023). In a typical solar installation, an inverter is used to convert the DC power to AC so that the energy generation can be used in a home. However, once this power is generated and distributed to a device, it must be converted back to DC at a device level. Thus, in recent years there has been increased interest in DC Microgrids as a method to deliver power more effectively. DC Microgrids allow for DC powered DERs to be coordinated together through a common DC bus, thus increasing the throughput of power from source to sink by removing unnecessary conversions between AC and DC power, resulting in up to 10-15% savings in overall system operation (Dragicevic, 2016 and Chauhan-1, 2018). DC Microgrids could be advantageous for residential adoption as noted in several studies which highlight that DC distribution has no inductive or capacitive losses, better voltage regulation, and reduced conductor resistance (Chauhan-2, 2018). In scenarios where there is a large adoption of renewable energy for power generation, DC Microgrids also provide a more resilient infrastructure due in part to the coordination of these DERs with an Energy Management System (EMS) that can seamlessly adapt to changing load conditions (Ali, 2021). However, due in part to the current lack of cohesive standards and high capital costs (Elsayed, 2014), DC Microgrids still have a long road of development before widespread adoption takes off. The transition to renewable energy and increasing electrification of everyday devices (heating, cooling, automotive, etc.) means that the electrical infrastructure must be rethought to accommodate these new loads.

What is the impact of running appliances on DC? It should be noted there are two main types of conversions between AC-DC and DC-AC power conversions: hard-switching and soft-switching. Hard-switching conversions typically operate in the range of 85-92% conversion efficiency, while soft-switching have efficiencies of 90-99% conversion efficiency (Mohammed, 2021). So, depending on the electrical distribution architecture, the throughput of power can be drastically diminished. Minimal studies are available which experimentally quantify the energy savings of running a base device on DC, but previous work has detailed that nearly all appliances can run on DC power and are often more efficient than their AC counterpart (Vossos, 2017). Vossos et al compared the nameplate energy efficiencies of products which offer both an AC and DC market-ready option and showed that DC counterparts were often 20-30% more efficient (Vossos, 2017). Many works which discuss the difference in efficiency of AC and DC appliances only do so with modeling estimates. The few experimental works which exist do so with small-scale appliances that operate at a nominally low voltage of 48VDC. The only previous experimental publication which compared an at-scale test of a residential heat pump was also done on the same 4-ton heat pump under current evaluation (Ore, 2020). This paper was limited to just cooling tests and did not evaluate the variable speed functionality of the heat pump. AHRI 210/240 test conditions were followed as detailed in the next section but the setpoint of the heat pump was set such that the unit was run at full speed across the tests but was not explicitly controlled. Under these conditions, there was a 6-8% increase in system COP with DC power. This paper serves as an extension of (Ore, 2020), whereby cooling and heating tests were performed under variable speed operation as shown in the next section.

This paper is thus divided into the following sections: methodology, results, discussion, and conclusion. The methodology section will outline the testing procedures followed as well as describe the thermodynamic model programmed into Engineering Equation Solver (EES) for data processing. The results section will concisely detail the test results on both AC and DC power input configurations. The discussion section serves to evaluate the test results and conceptually understand what causes the performance data difference between the power input configurations. The conclusion section will discuss ideas for future work and sum up the contributions of the present study.

2. METHODOLOGY

An off-the-shelf variable speed 4-ton residential heat pump split system with a scroll compressor was retrofitted to accept both AC and DC electrical supply inputs. The system is charged with 6.1 kg of R410a to achieve 5K of subcooling under the A2 conditions (Table 2) as per the manufacturer's specifications. The thermal system was left untouched, allowing for a straightforward performance comparison on the different power input configurations. Conventional residential AC power was supplied to the unit at a nominal split-phase 230VAC. The DC configuration operates at a nominal bi-polar 350VDC input with under and over voltage limits at 250 VDC and 400 VDC, respectively. Thermal and electrical performance is evaluated under variable speed operation using the AHRI 210/240 test procedures.

2.1 Description of Heat Pump Test Setup

The 4-ton residential unitary split system heat pump is situated in two psychrometric chambers which can precisely control the temperature and humidity to the required testing conditions (as discussed in section 2.2). Laboratory data is collected using a National Instruments cRIO-2091 data acquisition system (DAQ) with a LabVIEW visual interface for inspection and logging. Figure 1 provides a Piping and Instrumentation Diagram (P&ID) which details the location of thermocouple, pressure transducers, and a Coriolis mass flow meter in the refrigerant cycle for cooling mode. Although not given here, a similar P&ID can be established for heating mode as well. Table 1 provides accompanying state points for analysis of the cycle. Air data is collected using a 3x3 thermocouple grid at the inlet and outlet of the indoor unit and in this way an energy balance was corroborated between the refrigerant and air enthalpy methods as described in AHRI 210/240. A detailed description of the thermodynamic analysis is presented in section 2.3. The AHRI 210/240 test conditions were chosen since a variable speed heat pump system was tested. It should be noted that the vendor of the heat pump provided a proprietary testing controls board for specifying the RPM of each of the system's components: outdoor fan, indoor blower unit, and compressor speed. The controls board did not allow for interfacing to measure the RPM of the system's components, which is a limitation of the test procedure followed in this study. However, in determining the COP, EER, and SEER of the system, the RPM was not necessary.

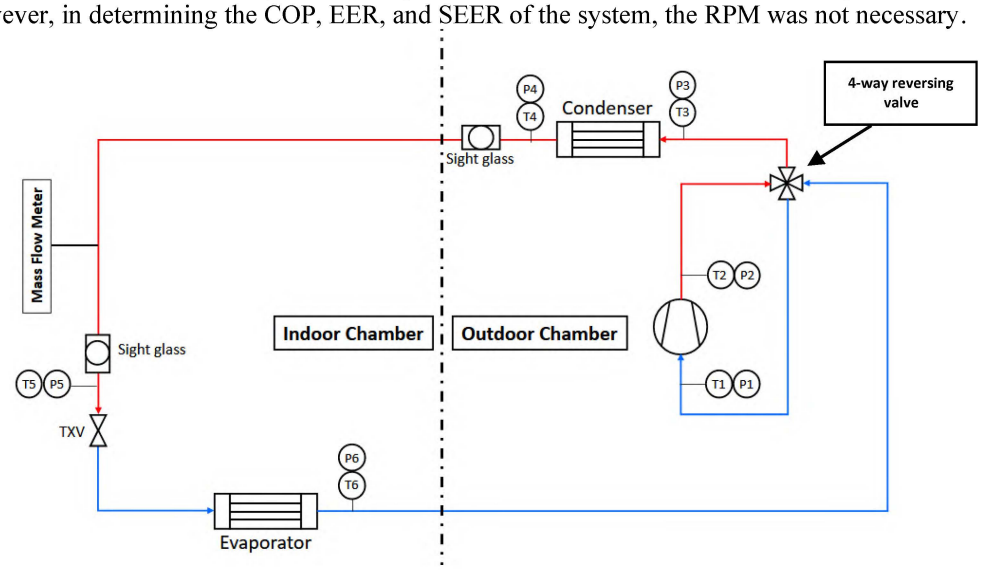

Figure 1: Piping and Instrumentation Diagram of the 4-ton Heat Pump cycle in Cooling Mode.

Table 1: State Point Descriptions and

State	Description	Measured/Calculated
1	Compressor Suction	Measured
2	Compressor Discharge	Measured
3	Condenser Inlet	Measured
4	Condenser Outlet	Measured
5	TXV Inlet	Measured
6	TXV Outlet	Calculated
7	Evaporator Inlet	Calculated
8	Evaporator Outlet	Measured

To measure the power that the system draws, two sets of watt transducers were required to gather data on the AC and DC configurations. The key difference between a DC and AC watt transducer is the current measurement method, which is either through a Hall effect sensor (DC) or an inductive measurement (AC). For the AC configuration, three inductive watt transducers were used to collect data from the total power to the indoor unit, the outdoor fan, and the compressor. The DC configuration uses two Hall-effect watt transducers to obtain the power consumed by the indoor and outdoor unit separately.

2.2 Description of AHRI 210/240 Tests

AHRI 210/240 specifies testing conditions for a variable speed unitary split system heat pump and is shown in Table 2. These conditions were replicated under both power input configurations to ensure commonality between testing

procedures. As can be seen, these test conditions go through a wide range of outdoor conditions and are standardized test conditions for evaluating the energy efficiency of equipment. The psychrometric chambers at Herrick Labs were used to achieve the test conditions by controlling each chamber's dry-bulb temperature and relative humidity.

Table 2: AHRI 210/240 Conditions for Variable Speed Cooling and Heating Tests

Test	Indoor Dry Bulb [°C]	Outdoor Dry Bulb [°C]	Indoor Relative Humidity [%]	Outdoor Relative Humidity [%]
A2	27	35	51	40
B2	27	28	51	40
B1	27	28	51	20
Ev	27	31	51	20
F	27	19	51	40
H01	21	17	56	72
H11	21	8	56	72
H1n	21	8	56	73
H2v	21	2	56	82
H32	21	-8	56	70

2.3 Thermodynamic Model of Setup

Thermophysical properties of R410a were calculated in EES (Klein, 2018). State points 1-5 were directly measured with pressure and temperature, and so their enthalpy can be calculated directly. The following assumptions were used: negligible pressure drop across the indoor unit coil, and isenthalpic expansion of the TXV. These assumptions allow for the calculation of the TXV outlet and the inlet to the indoor unit. The mass flow of the refrigerant was measured with a Coriolis mass flow meter as shown in Figure 1.

The cooling and heating capacity of the indoor heat exchanger was calculated via refrigerant and air enthalpy methods. These two methods were compared and maintained within 6% agreement to ensure accuracy of the system measurements. A First Law energy balance with the given assumptions gives the cooling and heating heat transfer as shown in Eq. 1. To determine the net cooling/heating capacity of the indoor heat exchanger, the work input to the blower was subtracted as shown in Eq. 2. The assumption being that the electric power delivered to the motor adds additional heat to the air.

$$\dot{Q}_{indoor} = \dot{m}(h_8 - h_7) \tag{1}$$

$$\dot{Q}_{net} = \dot{Q}_{indoor} - \dot{W}_{indoor} \tag{2}$$

The cooling and heating capacity is also calculated through an air enthalpy method. A First Law energy balance is analyzed on the indoor unit. The enthalpy change of the air is calculated, and in the case of cooling mode operation, the amount of water condensed out is also accounted for. This is summarized in Eq. 3. To calculate Eq. 3. the mass flow rate of the air passing over the heat exchanger must be accounted for as well. This is done by analyzing the volumetric flow rate of a nozzle box attached to the ducting of the indoor unit which is designed in compliance with ASHRAE Standard 37-2009 (ASHRAE, 2009). The volumetric flow rate of the air is calculated iteratively as shown in Eq. 4.

$$\dot{Q}_{air} = \dot{m}_{air}\Delta h - \dot{m}_{water}h_{water} \tag{3}$$

$$\dot{V}_{air} = Y\sqrt{\frac{2\Delta p_{nozzle}}{\rho_{air}}}\sum_{0}^{k} C_i A_i \tag{4}$$

ASHRAE Standard 37-2009 define the expansion factor (Y), as well as the coefficient of discharge (C_i), the area of the ductwork (A_i) was specified during system installation. Once the volumetric flow rate has sufficiently been

calculated, the mass flow rate of the air is simply calculated by multiplying the density of air with the volumetric flow rate as shown in Eq. 5.

$$\dot{m}_{air} = \dot{V}_{air}\rho_{air} \tag{5}$$

To calculate the phase change of water condensed out for cooling mode some combination of two of four measurements must be set: dry-bulb temperature, wet-bulb temperature, dew point, or relative humidity. At the inlet, the dry-bulb temperature is measured with a 3x3 thermocouple grid and the relative humidity is measured with a relative humidity sensor. At the outlet, the dry-bulb temperature is measured with a separate 3x3 thermocouple grid, and the dew-point is measured with a chilled mirror dew-point sensor sampled at 1 L/min. From these values, the change in enthalpy of the air is calculated and compared to within 6% agreement using the refrigerant enthalpy calculation. The Coefficient of Performance (COP) of the system is calculated as the ratio of the net cooling/heating capacity divided by the net power input to the system as shown in Eq. 6.

$$COP = \frac{\dot{Q}_{net}}{\dot{W}_{total}} \tag{6}$$

3. RESULTS

3.1 Steady State Results

Steady state performance results can be seen in Tables 3 and 4 which detail the thermal capacity delivered by the indoor unit as well as the power consumption of both the indoor and outdoor units. The COP is calculated per Eq. (5) and is listed as well.

Table 3: Steady State AC Test Results AHRI 210/240

Test	Thermal Capacity [kW]	Indoor Power [kW]	Outdoor Power [kW]	Total Power [kW]	COP [-]
A2	12.75	0.372	3.474	3.746	3.40
B2	13.78	0.211	3.038	3.155	4.36
B1	4.45	0.015	0.684	0.685	6.49
Ev	7.75	0.092	1.416	1.471	5.27
F	5.15	0.023	0.529	0.539	9.55
H01	4.30	0.072	0.660	0.705	6.09
H11	3.51	0.032	0.702	0.716	4.90
H1n	12.86	0.256	3.543	3.799	3.38
H2v	6.98	0.217	1.736	1.954	3.57
H32	10.32	0.572	4.292	4.865	2.12

Table 4: Steady State DC Test Results AHRI 210/240

Test	Thermal Capacity [kW]	Indoor Power [kW]	Outdoor Power [kW]	Total Power [kW]	COP [-]
A2	12.44	0.272	3.293	3.565	3.49
B2	13.60	0.204	2.840	3.044	4.47
B1	4.57	0.028	0.716	0.744	6.14
Ev	7.48	0.078	1.386	1.464	5.11
F	5.03	0.033	0.517	0.550	9.15
H01	4.58	0.084	0.665	0.749	6.11
H11	3.56	0.040	0.714	0.754	4.72
H1n	12.78	0.383	3.374	3.757	3.40
H2v	6.98	0.214	1.727	1.941	3.60
H32	10.49	0.544	4.241	4.785	2.19

Based on the results presented in Table 3, switching the HP to DC power provides a 2-3% improvement in system COP at full speed operation in cooling mode. However, the variable speed operation was 3-5% worse. In Table 4, switching the HP to DC power for heating mode provides marginal savings (< 1% improvement) at variable speed conditions. The full speed test at the coldest temperature (Test H32) showed the best improvement at +3.3% system COP. The low-speed heating test at a medium temperature (Test H11) showed the worst improvement at -3.7% system COP. These results are summarized by examining the trends in COP as a function of the steady state temperature lift as well as the percent improvement as a function of temperature lift across the test conditions as shown in Figure 2. There is an approximately linear trend in the percent improvement as a function of the temperature lift. This indicates that DC power provides better savings at full-load conditions, and worse performance at part-load conditions. It should again be noted that in general, based on the test conditions presented in Tables 3 and 4 the DC HP seems to operate more favorably in heating mode than cooling mode.

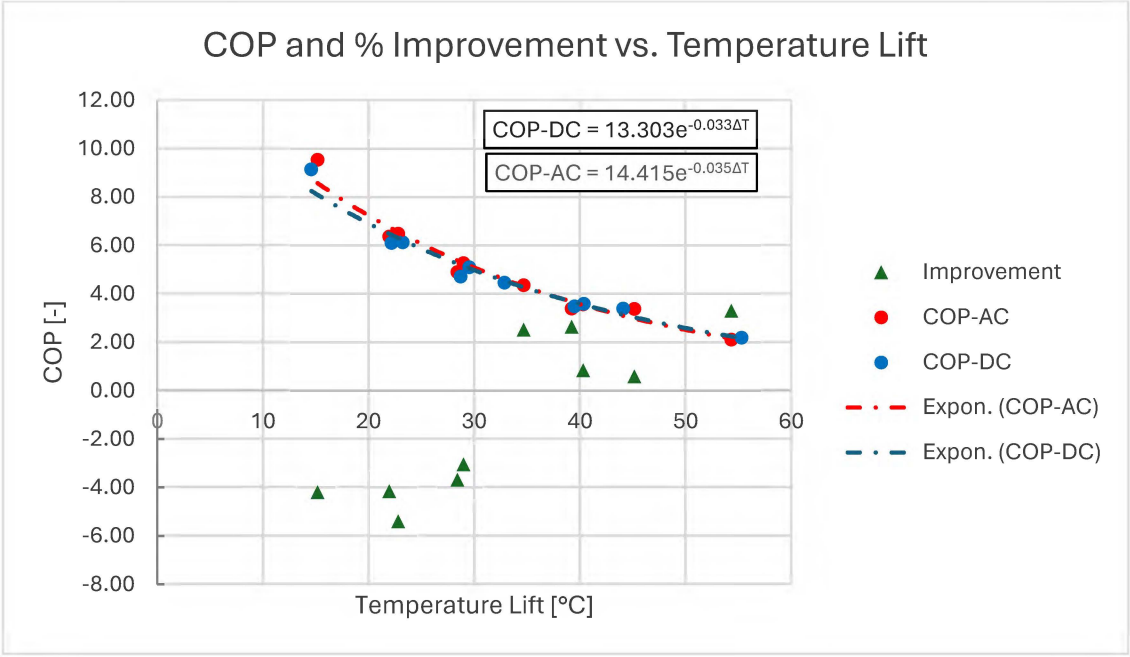

Figure 2: COP performance and COP improvement between AC and DC test conditions as a function of the steady state temperature lift.

Figures 3 and 4 show a P-h diagram plot overlaying the state point cycles of AC and DC power input configurations for both cooling (Fig. 3) and heating (Fig. 4) tests. Figure 2 shows the A2 cooling test conditions, and Figure 4 shows the H32 cooling test conditions. These test conditions were chosen as a case study since they are the largest thermal loads for cooling and heating on the system. In both figures, DC power is shown in blue and AC power is shown in red. The AC and DC test results in both heating and cooling show very similar state points for the cycle as can be seen. For the A2 cooling test in Figure 3, DC power resulted in slightly lower condensing and evaporating pressures, but still achieved similar thermal capacity. For the H32 heating test in Figure 4, the condensing pressure was identical, but the AC power input configuration resulted in a slightly lower evaporating pressure. The P-h plots were similar for all test conditions.

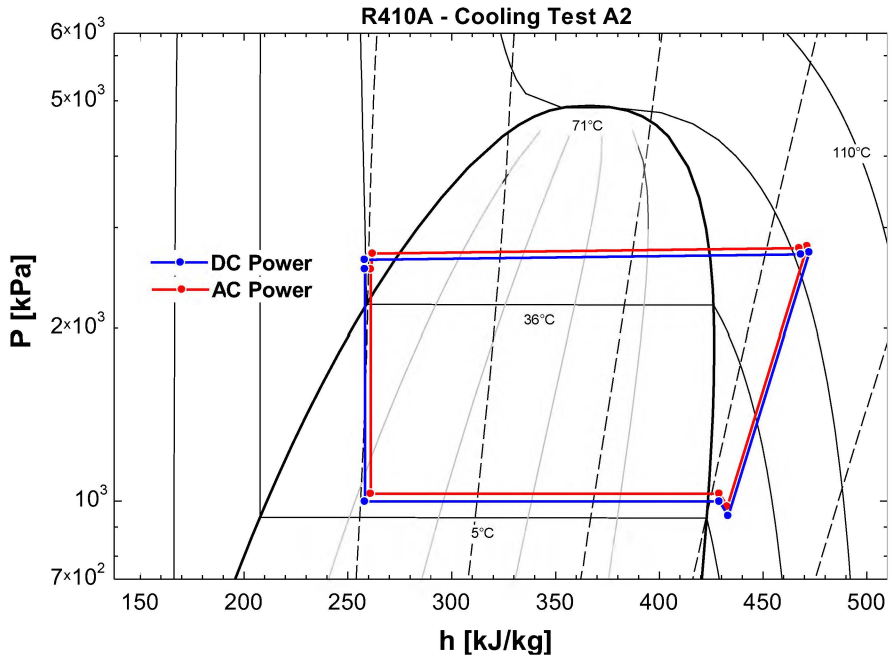

Figure 3: P-h diagram for the A2 test condition with state points drawn for AC/DC power configurations.

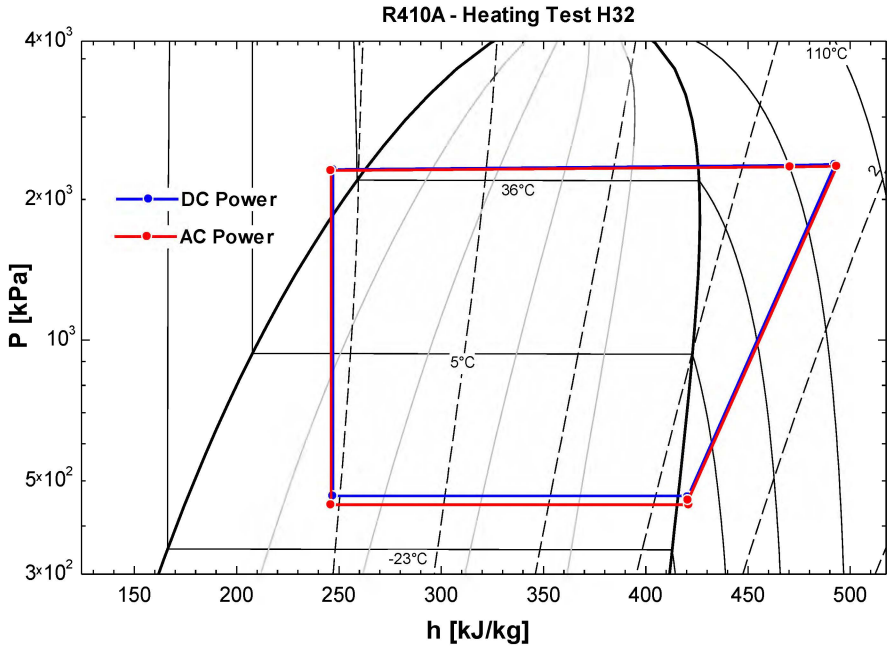

Figure 4: P-h diagram for the H32 test condition with state points drawn for AC/DC power configurations.

4. DISCUSSION

As seen in Tables 3 and 4, the thermal capacity of the system remained relatively unchanged from the different power input configurations. The results show that the DC power input configuration results in slightly worse performance at part-load conditions and increased performance at full-load conditions in both heating and cooling. Heating part load conditions result in similar performance between AC and DC power input. Cooling conditions saw the worst part load conditions. It is unclear precisely what may be causing this, but there are some likely culprits. In controlling all test conditions systematically so that the only true difference between operation in the preceding test results is the input of either AC or DC power, then performance differences must logically be localized to the motors. All motors of this system run on DC voltage, which means in the standard AC configuration that the power signal is rectified to the

proper DC signal for the motor. Therefore, the hypothesis is that if this rectifier is bypassed, then an improvement should be seen. The preceding test conditions did not have three DC power meters and so could not get granularity on the outdoor unit to differentiate between power consumed by the outdoor unit fan motor and the compressor's motor. Therefore, it would be useful in future work to distinguish the power consumption between the two so a better picture of the power consumption on DC versus AC can be established. It should be noted that the indoor power consumption had no discernible improvement or decrease. This is most likely due to the nozzle box which was used to set the indoor unit air flow rate and directly contributed to the power consumption of the blower. Thus, no strong conclusions can be made on its power consumption.

A sample rectifier circuit for a three-phase power input is shown in Figure 5. The AC signal goes through six diodes and is then rectified to a 350VDC signal. But when operating with DC, the power signal still needs to pass through the rectifier circuit, which means there is a small but not insignificant voltage drop across this rectifier circuit. For instance, if a diode is assumed to cause approximately 1V drop in a power circuit, then six diodes would cause a 6V drop. This means that the compressor's speed regulator is operating with a 344VDC Pulse Width Modulation signal and could be causing a different current draw for the compressor motor. Since there are coupled dynamics between the electromechanics of the motor, and the heat transfer and fluid properties of the compression chamber it is hypothesized in this paper that an in-depth coupled model between the rectifier circuit, the motor, and compression process is necessary to better understand the performance difference between AC and DC operation of a variable speed heat pump.

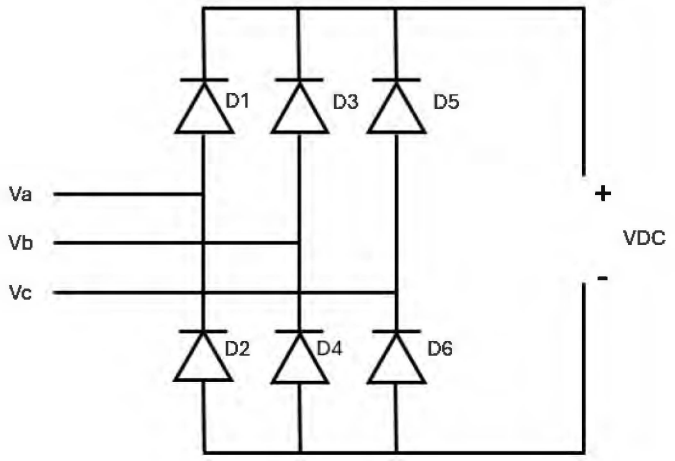

Figure 5: A sample 3-phase full bridge rectifier which converts an AC power input to a DC power output.

For future work it is thus recommended to develop a model which couples the rectifier, motor, and compression chamber and to use this paper's experimental results in its validation. To simplify experimental validation of the rectifier, motor, and compression chamber, the power electronics and compressor could be tested on a hot-gas bypass test stand to eliminate errors and to better measure the motor RPM, and electrical losses through a rectifier circuit. Future work should also experimentally assess the performance of a DC HP in a field test, such as the DC Nanogrid House so that seasonal performance can be calculated more accurately.

5. CONCLUSIONS

This work presented psychrometric testing results of a residential split system variable speed unitary heat pump operating under both AC and DC power inputs. AHRI 210/240 test conditions for heating and cooling in variable speed mode were used to properly compare the performance improvements by switching to DC power. This was done to quantify energy efficiency through bypassing conversions between AC and DC power as is traditionally done and to show what performance can be expected when operating a HP in a DC Nanogrid environment. The unit successfully functioned on a 350VDC input through all 10 test conditions as prescribed in Table 1. Based on the measurements and the analysis it was concluded that the performance improvement for DC power is linearly related to the steady state temperature lift of the cycle. In part load conditions (small temperature lift), the HP performed slightly worse on DC input. As the temperature lift increased, so did the performance of the HP at steady state conditions. It is not immediately clear what could potentially be causing this, and so it is recommended that future work is focused on

coupled modeling of the rectifier circuit, the compressor motor, and the compression chamber with experimental validation for system performance. Future work should also focus on field testing the variable speed system through a heating and cooling season to gain further insight.

NOMENCLATURE

AC	Alternating Current
AHRI	Air-Conditioning, Heating and Refrigeration Institute
ASHP	Air Source Heat Pump
COP	Coefficient of Performance
DAQ	Data Acquisition System
DC	Direct Current
DER	Distributed Energy Resource
DOE	Department of Energy
EES	Engineering Equation Solver
EIA	Energy Information Agency
HVAC	Heating, Ventilation and Air Conditioning
IEA	International Energy Agency
PV	Photo-Voltaic
RPM	Rotations Per Minute
US	United States
VAC	Voltage AC
VDC	Voltage DC
VPP	Virtual Power Plant

REFERENCES

Ali, S., Zheng, Z., Aillerie, M., Sawicki, J.-P., Péra, M.-C., & Hissel, D. (2021). A Review of DC Microgrid Energy Management Systems Dedicated to Residential Applications. *Energies*, *14*(14), 4308. https://doi.org/10.3390/en14144308

Chen, B., Wang, J., Lu, X., Chen, C., & Zhao, S. (2021). Networked Microgrids for Grid Resilience, Robustness, and Efficiency: A Review. *IEEE Transactions on Smart Grid*, *12*(1), 18–32. https://doi.org/10.1109/TSG.2020.3010570

Dong, D., Cvetkovic, I., Boroyevich, D., Zhang, W., Wang, R., & Mattavelli, P. (2013). Grid-Interface Bidirectional Converter for Residential DC Distribution Systems—Part One: High-Density Two-Stage Topology. *IEEE Transactions on Power Electronics*, *28*(4), 1655–1666. https://doi.org/10.1109/TPEL.2012.2212462

Dragicevic, T., Lu, X., Vasquez, J. C., & Guerrero, J. M. (2016). DC Microgrids—Part II: A Review of Power Architectures, Applications, and Standardization Issues. *IEEE Transactions on Power Electronics*, *31*(5), 3528–3549. https://doi.org/10.1109/TPEL.2015.2464277

Energy Information Agency (2023). Use of energy explained. *Energy Use in Homes,* https://www.eia.gov/energyexplained/use-of-energy/electricity-use-in-homes.php

Energy Information Agency (2023). U.S. construction costs dropped for solar, wind, and natural gas-fired generators in 2021. *Today in Energy,* https://www.eia.gov/todayinenergy/detail.php?id=60562

Elsayed, A. T., Mohamed, A. A., & Mohammed, O. A. (2015). DC microgrids and distribution systems: An overview. *Electric Power Systems Research*, *119*, 407–417. https://doi.org/10.1016/j.epsr.2014.10.017

Mohammed, S. A. Q., & Jung, J.-W. (2021). A State-of-the-Art Review on Soft-Switching Techniques for DC–DC, DC–AC, AC–DC, and AC–AC Power Converters. *IEEE Transactions on Industrial Informatics*, *17*(10), 6569–6582. https://doi.org/10.1109/TII.2021.3058218

Ore, J., Meral, F., Obst, O., Kurtulus, O., & Groll, E. A. (2020). *Evaluation of a Hybrid AC/DC Powered Residential Split- System Heat Pump Performance using a DC Nanogrid*.

Downing, J., Johnson, N., McNicholas, M., Nemtzow, D., Oueid, R., Paladino, J., Wolfe, E.B., U.S. Department of Energy (2023). *Pathways to Commercial Liftoff: Virtual Power Plants*. (n.d.).

Shahidehpour, M., Liu, X., Li, Z., & Cao, Y. (2016). Microgrids for Enhancing the Power Grid Resilience in Extreme Conditions. *IEEE Transactions on Smart Grid*, 1–1. https://doi.org/10.1109/TSG.2016.2579999

ACKNOWLEDGEMENT

The authors would like to extend gratitude to the Center for High Performance Buildings (CHPB) at Herrick Labs for their funding of this project. Trane Technologies was very influential for technical feedback and help throughout this study, John Hughes for electrical expertise, and Jason LeRoy for thermal engineering help. The authors also extend gratitude to Jan Spale who was vital for help in understanding the outcome of the study and interpreting results. The authors would also like to sincerely thank Frank Lee, Jose Lopez, and Cody Bahler for their extensive help throughout this project. Without excellent technicians working in the lab, this study could not have been possible to accomplish.